


Research Article

Experimental Study of the Dynamic Shear Modulus Ratio and Damping Ratio of the Quaternary Sedimentary Soils in the Offshore Areas of the Yellow Sea

Yi Fang,¹ Yuejun Lv,¹ Dandan Xu,² Yanju Peng ,¹ and Xingyuan Zhou¹

¹National Institute of Natural Hazards, Ministry of Emergency Management of China, Beijing 100085, China

²Beijing Geotechnical Institute Engineering Consultants Ltd., Beijing 100038, China

Correspondence should be addressed to Yanju Peng; pengyj408@126.com

Received 22 May 2021; Revised 7 August 2021; Accepted 6 September 2021; Published 30 September 2021

Academic Editor: Huie Chen

Copyright © 2021 Yi Fang et al. This is an open access article distributed under the Creative Commons Attribution License, which permits unrestricted use, distribution, and reproduction in any medium, provided the original work is properly cited.

The effects of marine and continental sedimentary environments and geological ages on the dynamic shear modulus ratio and damping ratio of the Quaternary sedimentary soils in the offshore areas of the Yellow Sea were analyzed by using a resonant column device (GCTS, USA). The results show the following: (1) The G_{\max} of various marine soils increases with the depth and shows a typical linear relationship. (2) The marine transgression has significantly different effects on the dynamic shear modulus ratio versus the shear strain amplitude curves (i.e., $G/G_{\max} \sim \gamma_a$ curves) and the damping ratio versus the shear strain amplitude curves (i.e., $\lambda \sim \gamma_a$ curves) of the different soil types in the offshore areas of the Yellow Sea. The effects of marine transgression were strong on clays, moderate on silty clays, and minor on silts. (3) The geological ages have noticeable effects on the $G/G_{\max} \sim \gamma_a$ curves of the tested marine silty clays, marine silts, and continental silty clays, but the effects of geological ages on the $\lambda \sim \gamma_a$ curves are minimal. The fitting parameters and recommended empirical equations of the $G/G_{\max} \sim \gamma_a$ and $\lambda \sim \gamma_a$ curves for each type of the tested soils (silty clay, clay, and silt) were obtained mirroring the effects of sedimentary environments and geological ages.

1. Introduction

The 21st century is widely considered to be the era of the ocean. All of the coastal countries have placed a higher priority on the ocean within their overall framework of national development. China has a very long coastline of more than 18,000 km, and thus, China has successively proposed marine strategic plans such as the Belt and Road and the Yellow Sea Economic Circle. In particular, the Yellow Sea and its coastal areas are experiencing intensive planning and construction of a large number of offshore traffic projects and marine projects. The Yellow Sea and its coastal areas are located in the North China Seismic Zone, which has complex seismic geological structures and is frequently subject to seismic activity, including a magnitude 6 earthquake in the Yellow Sea in 1764, a magnitude 6.5 earthquake in the Yellow Sea in 1764, and a

far-field magnitude 8.5 earthquake in Tancheng in 1668. There may be Late Pleistocene faults and Holocene faults in the zone, which increase the possibility of destructive earthquakes in the future. The offshore areas of the Yellow Sea contain a thick Quaternary sedimentary sequence, which is comprised of soft soils. These soils are mainly marine plains dominated by cohesive soils and saturated sandy soils. The strong earthquakes that occur in this area may lead to a significant site amplification effect and result in the subsidence of soft soil or liquefaction of sandy soil in these areas, which poses a serious threat to the safety of major engineering structures and the performance of socioeconomic activities.

The variation of the dynamic shear modulus ratio G/G_{\max} and the damping ratio λ against the shear strain amplitude γ_a directly reflects the nonlinear and hysteretic characteristics of the stress-strain relationship of soils under

dynamic loads. They are not only the basic dynamic parameters to describe the nonlinear hysteretic constitutive model but also essential for accurately analyzing the seismic response of soil layers.

The G/G_{\max} and λ of soils are strongly region-specific since soils in different regions might be from different geological ages, exist in different sedimentary facies, and have different sedimentogenesis [1–6]. At present, a large number of studies have been carried out on marine soils. For example, Koutsoftas and Fischer explored the influence of the overconsolidation ratio OCR on the dynamic characteristics of G and λ of two kinds of marine clays through resonance column and cyclic triaxial tests [7]. Liang et al. proposed a new correlation function method for the calculation of G and λ in triaxial tests and investigated the $G/G_{\max} - \gamma_a$ and $\lambda - \gamma_a$ curves of saturated coral sand from the Nansha Islands, South China Sea, considering the influence of effective confining pressure and relative density [8]. Yang et al. established the empirical equations of $G/G_{\max} - \gamma_a$ curves for the undisturbed soils in the Yangtze River estuary [9]. Morsy et al. evaluated the dynamic characteristics of Egyptian calcareous sand in the range of small and medium shear strains [10]. Wu et al. researched the small-strain stiffness of marine silty sand [11]. Senetakis and Payan conducted small-strain resonant column tests in torsional and flexural modes of vibration which quantified two types of damping ratios [12]. Some tests have been conducted for the dynamic characteristics of fine-grained soil, especially for high plasticity clay [13]. Based on field and laboratory tests, researchers studied the static and dynamic properties of soils in Catania [14]. Głuchowski et al. researched the laboratory characterization of a compacted-unsaturated silty sand. The results proposed that the compaction procedure caused an overconsolidation state dependent on the moisture content during compaction effort [15]. Feng et al. used the resonance column test to evaluate the influence of confining pressure, mix ratio, curing age, and cement content on the dynamic characteristics of subsea sand-silt mixtures [16]. Khosravi et al. developed a new methodology to extend an existing small-strain shear modulus G_{\max} model to determine G_{\max} of unsaturated silty soils along different paths of the soil water retention curve including the scanning loops [17].

However, few tests pay attention to the influence of sedimentary environment and geological age on the dynamic properties of soil, especially if they had significant impact on dynamic shear modulus ratios and damping ratios. Furthermore, the experimental studies on the G and λ characteristics of the soils in the coastal area of the Yellow Sea have not been reported yet.

To fill this knowledge gap, in this study, the dynamic shear modulus ratios and damping ratios of the soils in a typical region of the coastal areas of the Yellow Sea are tested by resonant column tests. The effects of sedimentary facies and geological ages were explored in detail. The results of this study provide a scientific and theoretical basis to analyze seismic site effects for major engineering sites.

2. Engineering Geological Conditions of the Study Region

The study area is located near the coast of the Yellow Sea, and most parts of the region are less than 5 m above sea level, falling in the category of a coastal marine plain. The Quaternary sediments in the region are more than 200 m thick and have experienced marine transgression five times since the late Early Pleistocene. With the formation of fluvial, lacustrine, and marine deposits alternately, broad coastal facies and alluvial facies with soft clay layers and saturated sand layers have been formed.

According to the chronological order of strata, the characteristics of soil sedimentary structure are as follows:

- (1) During the Holocene period, the stratum was buried at a depth of 8–25 m, mainly composed of tidal flat facies of clay, clay interbedded with silt, silt and clay interbedded, and gray clay
- (2) In the Late Pleistocene, the stratum was buried at a depth of 16–21 m, mainly composed of gray clay and silt flooding facies and gray lacustrine deposits
- (3) In the early Late Pleistocene, the stratum was buried at a depth of 28–42 m, mainly composed of tidal flat facies of gray clay, clay intercalated with silt sand, clay silt sand, and gray clay supertidal zone deposits
- (4) In the late Middle Pleistocene, the stratum was buried 40–55 m deep and 7–20 m thick. The lower part mainly was composed of flooding facies and high tide flats, and the upper part was composed of lacustrine facies
- (5) In the early mid-Pleistocene, the stratum was buried 70–106 m deep and 25–60 m thick. The lower part was composed of gray clay lagoon facies and tidal flat facies, partially with gray-green fine sand in riverbed facies and gray silt delta facies, and the upper part was composed of tidal flat facies and shallow ocean facies with gray clay and silt sand

The sedimentary environments and geological ages of the soils have a significant impact on their dynamic deformation characteristics. The soil samples were identified based on their colors and the existence of shells, calcareous nodules, and iron-manganese oxides. The identifications in conjunction with the comparison between the borehole logs and the relevant geological maps account for the classification of soil categories, sedimentary facies, and geological ages of the tested samples. The classification, summarized in Table 1, reveals that there are 19 clayey soil samples in the shallow layers, within 100 m below the surface. 75% of the silt samples are mainly deposited in the Pleistocene, which is attributed to the fact that the seawater in the marine transgression carried a large amount of granular soils from the rivers, lakes, and marine facies into the flat areas where separation and sedimentation took place. The Holocene silt sand samples are mainly deposited in the marine facies. The silty clay samples from both the marine and continental

TABLE 1: Basic physical properties of undisturbed soil.

Number	Lithology	Depth, h (m)	Consolidation pressure, σ' (kPa)	Density, ρ (g/cm ³)	Moisture content, ω (%)	Void ratio, e	State
1	Silty clay	51.7-52.0	345	2.09	22.77	0.53	CL
2	Clay	80.7-81	540	2.10	30.75	0.70	ML
3	Silty clay	3.7-4.0	50	1.85	34.46	0.91	CH
4	Silty clay	17.0-17.3	115	1.95	33.14	0.81	CL
5	Silty clay	21.5-21.8	145	1.87	27.03	0.77	CL
6	Clay	39.8-40	265	1.96	29.53	0.79	CL
7	Silty clay	50.1-50.3	335	2.02	23.44	0.63	CL
8	Silty clay	54-54.3	360	1.94	27.53	0.72	CL
9	Clay	79.8-80.0	535	2.06	23.40	0.55	CL
10	Clay	94.6-94.8	635	2.01	29.50	0.69	CL
11	Silty clay	3.0-3.3	50	1.84	30.79	0.90	CH
12	Silty clay	17.0-17.3	115	1.81	33.38	0.95	CL
13	Silty clay	18.7-19.0	125	1.96	29.73	0.79	CL
14	Silty clay	17.05-17.25	115	2.06	25.87	0.60	CL
15	Clay	34.05-34.25	230	2.13	24.54	0.52	CL
16	Clay	44.05-44.25	295	2.03	25.74	0.74	CL
17	Silty clay	54.05-54.25	360	2.03	22.03	0.57	CL
18	Clay	76.85-77.05	515	1.99	26.56	0.70	ML
19	Silty clay	17.2-17.4	115	2.11	24.89	0.58	CL
20	Silty clay	23.5-23.7	160	1.89	33.97	0.93	CH
21	Clay	27.6-27.8	185	2.14	23.55	0.50	CL
22	Silty clay	40.2-40.4	270	1.98	24.34	0.68	CL
23	Clay	77.3-77.5	515	2.03	25.56	0.64	CL
24	Clay	97.8-98	655	2.12	27.36	0.63	ML
25	Silty clay	33.7-34	225	1.95	40.32	0.92	CL
26	Clay	71.8-72	480	2.09	29.78	0.66	ML
27	Clay	78.7-79	525	2.13	24.91	0.58	ML
28	Silty clay	5.8-6	50	1.84	38.55	0.94	CH
29	Silty clay	12.8-13	85	1.91	33.45	0.88	CL
30	Clay	35-35.3	235	1.95	21.59	0.67	CL
31	Silty clay	40-40.3	270	1.94	26.84	0.72	CL
32	Silty clay	47.7-48	320	1.98	25.87	0.72	CL
33	Silty clay	57.7-58	385	1.98	25.51	0.68	CL
34	Clay	64-64.3	430	1.96	38.04	0.85	ML
35	Clay	79-79.3	530	2.01	26.76	0.68	ML
36	Clay	83-83.3	555	1.99	27.45	0.69	ML
37	Clay	86.4-86.7	580	2.03	25.56	0.66	CL
38	Clay	89.7-90	600	2.06	20.46	0.57	ML
39	Clay	92.7-93	620	2.10	21.76	0.55	ML
40	Silty clay	4-4.2	50	1.87	34.54	0.84	CL
41	Silt	14.8-15	100	1.96	30.56	0.81	Medium
42	Silty clay	30-30.2	200	1.97	22.56	0.66	ML
43	Silt	36.8-37	245	2.01	29.45	0.70	Dense
44	Silt	42.8-43	285	1.99	30.12	0.75	Dense
45	Silt	50.8-51	340	2.03	28.15	0.69	Dense
46	Silty clay	70-70.2	470	2.10	23.56	0.59	ML
47	Silty clay	78-78.2	520	1.99	23.45	0.68	ML
48	Silt	86.6-87	580	2.06	28.23	0.67	Dense

TABLE 1: Continued.

Number	Lithology	Depth, h (m)	Consolidation pressure, σ' (kPa)	Density, ρ (g/cm ³)	Moisture content, ω (%)	Void ratio, e	State
49	Silty clay	93-93.2	620	2.08	23.76	0.59	ML
50	Silt	5.5-5.7	50	1.93	31.67	0.81	Medium
51	Silty clay	11.5-11.7	80	1.96	24.56	0.70	CL
52	Silt	22-22.2	150	1.98	29.98	0.79	Medium
53	Silty clay	32-32.2	215	1.96	23.45	0.66	ML
54	Silt	54-54.2	360	1.99	29.23	0.76	Dense
55	Silty clay	77-77.2	515	2.03	24.87	0.62	ML
56	Silt	88-88.2	590	2.02	30.21	0.73	Dense
57	Silty clay	96-96.2	640	2.08	21.87	0.55	ML
58	Silty clay	7-7.2	50	1.86	32.76	0.89	CL
59	Silt	13-13.2	90	1.94	28.23	0.81	Medium
60	Silty clay	21.5-21.7	145	1.95	27.89	0.71	CL
61	Silty clay	35-35.2	235	2.04	23.87	0.63	ML
62	Silt	45.5-45.7	305	2.05	29.87	0.70	Dense
63	Silty clay	63.5-63.7	425	2.03	21.89	0.62	ML
64	Silt	80-80.2	535	2.02	26.97	0.72	Dense
65	Silty clay	98.5-98.7	660	2.11	20.21	0.56	ML
66	Silty clay	8-8.2	55	1.92	31.98	0.79	CL
67	Silt	18.8-19	125	1.98	32.87	0.80	Medium
68	Silty clay	30-30.2	200	1.96	19.87	0.61	ML
69	Silt	40.8-41	275	1.97	29.76	0.77	Dense
70	Silt	57-57.2	380	2.00	26.89	0.73	Dense
71	Silt	68.8-69	460	2.01	28.98	0.73	Dense
72	Silt	83.8-84	560	2.04	27.12	0.70	Dense
73	Silty clay	92-92.2	615	2.11	18.12	0.53	ML
74	Silt	5.8-6.0	50	1.98	33.80	0.81	Medium
75	Silty clay	11-11.2	75	1.95	24.21	0.69	CL
76	Silt	21.8-22	145	1.97	30.12	0.77	Medium
77	Silty clay	35-35.2	235	1.95	29.87	0.77	Medium
78	Silty clay	44-44.2	295	1.98	25.12	0.69	CL
79	Silt	52.8-53	355	1.99	28.98	0.74	Dense
80	Silty clay	74-74.2	495	2.01	19.21	0.61	ML
81	Silty clay	93-93.2	620	2.01	20.21	0.60	ML
82	Silty clay	9-9.2	60	1.89	31.23	0.85	CL
83	Silty clay	27-27.2	180	1.93	24.32	0.71	CL
84	Silty clay	37-37.2	250	1.99	25.21	0.67	ML
85	Silty clay	47-47.2	315	1.96	25.90	0.70	CL
86	Silty clay	58.5-58.7	390	2.03	21.23	0.60	ML
87	Silty clay	70-70.2	470	2.07	23.21	0.62	ML
88	Silty clay	83.5-83.7	560	2.12	21.32	0.55	ML
89	Silty clay	98-98.2	655	2.11	22.87	0.58	ML

facies were primarily deposited in the Holocene and Pleistocene.

3. Soil Sampling and Testing

3.1. Soil Sampling. A total number of 89 undisturbed soil samples were collected from 14 boreholes in the coastal area

of the Yellow Sea by using the in situ soil tube method. The depth of soil samples are from 0 to 100 m. As shown in Figure 1, the borehole sites were distributed close to each other so as to reveal the dynamic characteristics of the soils in more detail. Each undisturbed soil sample was prepared into a solid cylindrical shape specimen with the diameter of 50 mm and the height of 100 mm.



FIGURE 1: Location of the boreholes in the offshore of the Yellow Sea.

3.2. Resonant Column Testing. The testing was conducted using the TSH-100 high-precision fixed-free resonant column device (GCTS, USA) at the Institute of Natural Disaster Prevention and Control of the Ministry of Emergency Management (Figure 2). The torque (or rotation) and the cell pressure are controlled independently by the apparatus. The consolidation pressure is provided by a pneumatic servo system, and a fully automated floating torsional drive is attached to excite at the top of the samples.

First, the soil was made into a solid cylindrical sample with a diameter of 50 mm and a height of 100 mm. Isotropic consolidation was conducted after the soil specimen was installed into the test apparatus, with a membrane filmed outside it. The effective confining pressure was determined according to the depth of the soil layer. The durations of the consolidation are more than 3 hours and 12 hours for cohesionless soils and cohesive soils, respectively. After consolidation, resonant column testing was conducted by applying the multistage frequency sweeping excitation on the top of the specimen following ASTM D4105-92 to measure the shear modulus G and damping ratio λ in the shear strain range of 10^{-6} ~ 10^{-3} . The schemes of the resonant column tests, specifically the index properties of the specimens and the corresponding effective confining pressures, are listed in Table 1.

4. Testing Results and Analysis

Since the sedimentary environment and geological age of the soils have a significant impact on their dynamic shear modulus ratios and damping ratios, the soil samples were observed to determine their colors and whether or not they contained shells, calcareous nodules, and/or iron-manganese oxides. The observations were made in conjunction with the comparative analysis of the borehole logs and the relevant geological maps in order to categorize the soil samples based on their soil properties, sedimentary facies, and geological ages. The results (Table 2) revealed that there were many clayey soils in the shallow layers within 100 m of the surface, while the silt samples were mainly deposited in the Pleistocene, which is attributed to the fact that the seawater in the marine transgression carried a large amount of gravel soils from the rivers, lakes, and marine facies into the flat areas where separation and sedimentation took place. In contrast, the silty clay samples from both the marine and continental facies were primarily deposited in the Holocene and Pleistocene. The Holocene clay samples were mainly deposited in the marine facies.

Figure 3 shows the typical results of the resonant column test. The strain amplitude of the sample under different excitation frequencies is shown in Figure 3(a). The resonance frequency f_1 of the sample γ_a at the maximum under the

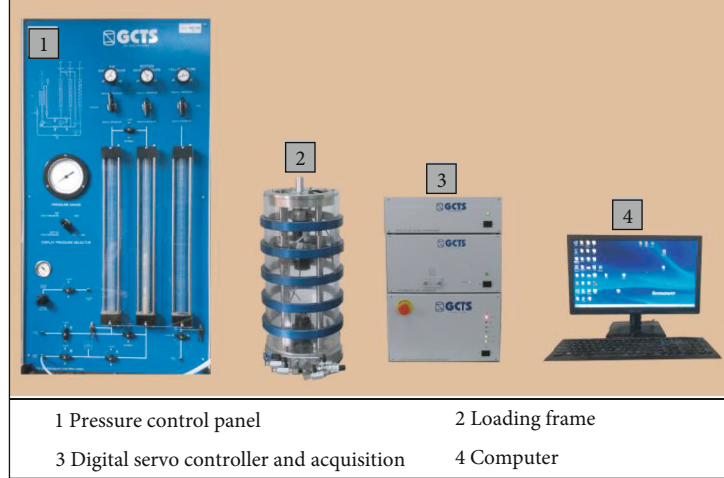


FIGURE 2: TSH-100 resonant column testing system.

TABLE 2: Classification and the corresponding number of the tested soil samples.

Lithology	Sedimentary environment	Geological age	
		Holocene	Pleistocene
Silt clay	Marine	11	15
	Continental	6	19
Silt sand	Marine	5	9
	Continental	0	6
Clay	Marine	0	9
	Continental	0	10

corresponding excitation load can be obtained. At the resonance frequency, the strain time history of the sample is shown in Figure 3(b). Under free vibration, the strain time history of the sample is shown in Figure 3(c).

4.1. Change of G_{\max} with Depth. As an important parameter for evaluating the dynamic characteristics of soil and characterizing the maximum elastic stiffness of soil, the maximum dynamic shear modulus G_{\max} is usually defined as G when $\gamma_a \leq 10^{-6}$. According to the hyperbolic relationship between soil dynamic modulus and dynamic strain under small vibration proposed by Hardin and Drnevich [18], the linear relationship between $1/G$ and γ_a can be obtained as $1/G = a + b\gamma$. And then, the hyperbolic model ($\gamma_a \rightarrow 0$) between $1/G$ and shear strain γ_a can be used to obtain the maximum dynamic shear modulus G_{\max} of marine soil.

$$G_{\max} = \lim_{\gamma \rightarrow 0} \frac{1}{a + b\gamma}. \quad (1)$$

The TSH-100 resonant column test system developed by the GCTS company can measure the dynamic shear modulus G of the soil in the range of $10^{-6} \sim 10^{-3}$. Equation (1) can be used to obtain the G_{\max} of marine soil at different depth ranges from 15 to 140 MPa.

Figure 4 shows the G_{\max} values of various marine soils and their changes with depth. It can be seen that the G_{\max} of various marine soils increases with the depth and shows a typical linear relationship. The prediction relationship between G_{\max} and depth can be expressed as $G_{\max} = 15.37 \times h + 1.13$. The h represents the depth of the sample, and its unit is m.

4.2. Effects of the Sedimentary Environment on the $G/G_{\max} \sim \gamma_a$ and $\lambda \sim \gamma_a$ Curves. The three-parameter Martin-Davidenkov model was adopted to investigate the variation characteristics of dynamic shear modulus ratio G/G_{\max} against the shear strain amplitude γ_a of the tested soils since it has been proven to fit experimental data well for soil samples in Jiangsu province, China [5]. The model is expressed as

$$\frac{G}{G_{\max}} = 1 - \left[\frac{(\gamma/\gamma_0)^{2B}}{1 + (\gamma/\gamma_0)^{2B}} \right]^A. \quad (2)$$

Here, A , B , and γ_0 are the best-fitting parameters. In particular, in the case of $A = 1$ and $B = 0.5$, the Martin-Davidenkov model simplifies to the H-D hyperbolic model [19], where γ_0 denotes the reference shear strain and is equal to the shear strain values when $G/G_{\max} = 0.5$ [20].

The damping ratio versus shear strain amplitude ($\lambda - \gamma_a$) curves of each tested specimen were fitted and analyzed using the following empirical Equation (3) proposed by Chen et al. [5]:

$$\lambda = \lambda_{\min} + \lambda_0 \times \left(1 - \frac{G}{G_{\max}} \right)^\beta. \quad (3)$$

Here, λ_{\min} is the basic damping ratio of a soil sample under a very small strain, which is related to the soil properties and consolidation state. λ_0 and β are the shape coefficients of the $\lambda - \gamma_a$ curve.

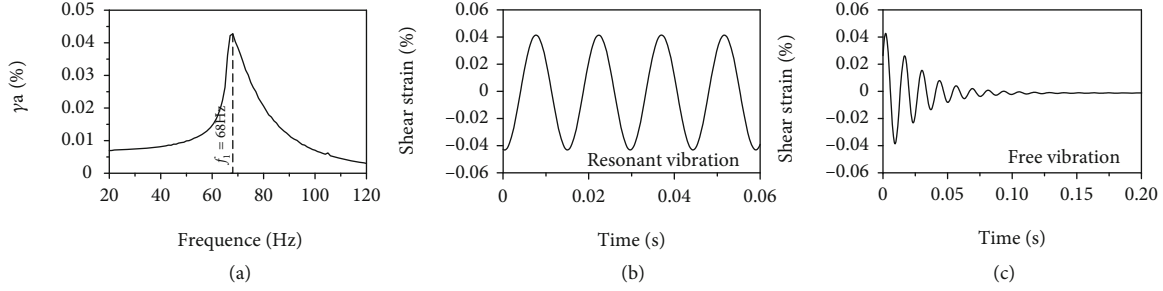


FIGURE 3: Typical results of resonant column test.

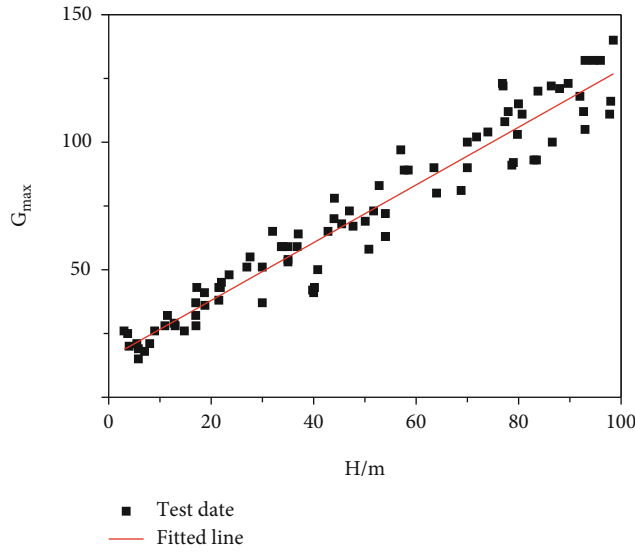


FIGURE 4: Variation relationship of the maximum dynamic shear modulus G_{max} with depth.

Figure 5 illustrates the effects of marine and continental sedimentary environments on the $G/G_{max} \sim \gamma_a$ and $\lambda \sim \gamma_a$ curves for the various types of soils. For Holocene silty clays, the $G/G_{max} \sim \gamma_a$ curves of the marine silty clays are slightly lower than those of the continental silty clays, while the $\lambda \sim \gamma_a$ curves of the marine silty clays are higher than those of the continental silty clays. This is mainly attributed to the fact that the marine silty clays were dominated by muddy silty clay deposited during the Holocene, and therefore, they exhibit stronger nonlinearity. For Pleistocene clays, the $G/G_{max} \sim \gamma_a$ curves of the marine clays are higher than those of the continental clays, while the $\lambda \sim \gamma_a$ curves of the marine clays are lower than those of the continental clays, which may be due to the higher strength of the clay crust formed during the marine transgression. The differences between the marine and continental silty clays in terms of their $G/G_{max} \sim \gamma_a$ and $\lambda \sim \gamma_a$ curves are smaller than the differences between the marine and continental clays. The $G/G_{max} \sim \gamma_a$ curves of the marine silty clays are slightly lower than those of the continental silty clays, while the marine and continental silty clays have similar $\lambda \sim \gamma_a$ curves. For the Pleistocene silt sands, the marine $G/G_{max} \sim \gamma_a$ and $\lambda \sim \gamma_a$ curves are similar to the continental $G/G_{max} \sim \gamma_a$ and $\lambda \sim \gamma_a$ curves. In general, within the working range of the shear strain ($10^{-6} \sim 10^{-3}$) of the resonant column device, the $G/G_{max} \sim \gamma_a$ curves of

the marine soils are slightly higher than those of the continental soils, and the differences between the $\lambda \sim \gamma_a$ curves of the two types of soils are even smaller.

4.3. Effects of Geological Age on the $G/G_{max} \sim \gamma_a$ Curve and $\lambda \sim \gamma_a$ Curves. Due to the limited number of sampling sites, the Pleistocene soils were not further classified into different Pleistocene stages. The $G/G_{max} \sim \gamma_a$ and $\lambda \sim \gamma_a$ curves of the various soil types were compared considering the two geological age categories: the Pleistocene versus the Holocene (Figure 6). The results show that in general, the geological age strongly affects the $G/G_{max} \sim \gamma_a$ and $\lambda \sim \gamma_a$ curves of the marine soils (silt clays and silt sands). The $G/G_{max} \sim \gamma_a$ curves of the Pleistocene marine soils are higher than those of the Holocene marine soils while the $\lambda \sim \gamma_a$ curves of the Pleistocene marine soils are lower than those of the Holocene marine soils. For continental depositional, geological age has a clear effect on the $G/G_{max} \sim \gamma_a$ curves of the continental silt clays. The $G/G_{max} \sim \gamma_a$ curves of the Pleistocene continental silt clays are significantly higher than those of the Holocene continental silt clays. However, the effect of geological age on the $\lambda \sim \gamma_a$ curves is quite weak. Overall, geological age has less effect on the $\lambda \sim \gamma_a$ curves of the continental soils than those of the marine soils.

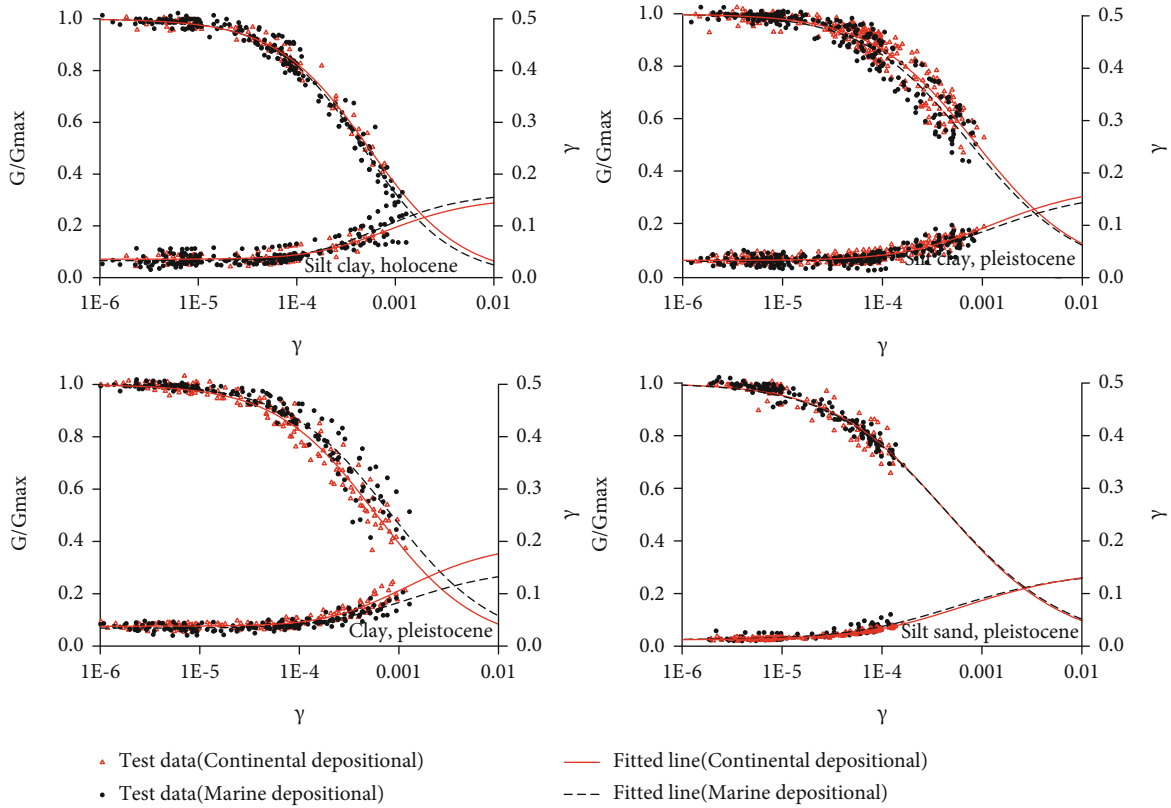


FIGURE 5: Comparison of $G/G_{max} \sim \gamma_a$ curve and $\lambda \sim \gamma_a$ fitting curves between marine deposit and continental deposit.

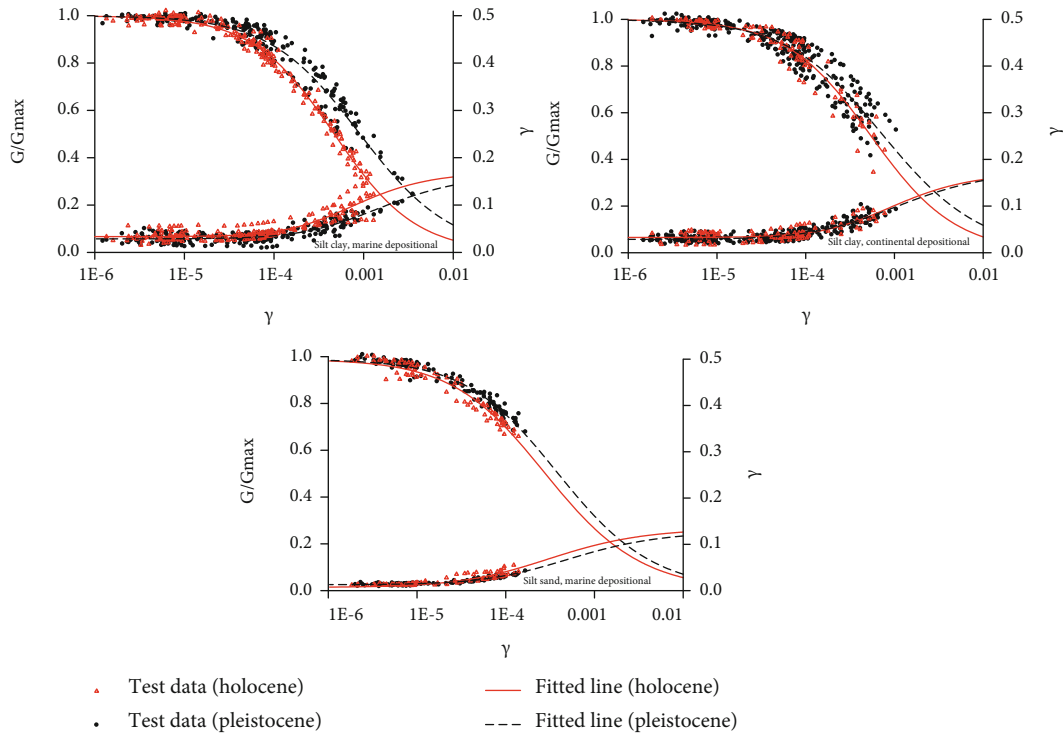


FIGURE 6: Influence of geological age on $G/G_{max} \sim \gamma_a$ curve and $\lambda \sim \gamma_a$ fitting curves of different deposits.

TABLE 3: Recommended parameter values for $G/G_{\max} - \gamma_a$ and $\lambda - \gamma_a$ curves of Quaternary sedimentary soils in the offshore areas of the Yellow Sea.

Lithology	Geological age/deposit	Number of samples	Fitting parameters					
			A	B	$\gamma_0 (10^{-4})$	λ_{\min}	λ_0	β
Silt clay	Holocene	17	1.01	0.48	4.77	0.034	0.132	1.477
	Pleistocene	34	1.12	0.40	6.93	0.029	0.136	1.363
Silt sand	Holocene	5	1.15	0.39	2.22	0.007	0.127	1.085
	Pleistocene	15	1.17	0.39	3.01	0.013	0.115	1.226
Clay	Continental depositional	10	1.05	0.42	5.52	0.038	0.161	1.732
	Marine depositional	9	1.09	0.41	7.32	0.034	0.116	1.376

TABLE 4: Average values of G/G_{\max} and λ at various shear strain levels for Quaternary sedimentary soils in the offshore areas of the Yellow Sea.

Lithology	Geological age/deposit	Parameters	Shear strain (10^{-4})							
			0.05	0.1	0.5	1.0	5.0	10	50	100
Silt clay	Holocene	G/G_{\max}	0.9883	0.9774	0.9004	0.8220	0.4933	0.3328	0.0958	0.0516
		λ (%)	3.39	3.42	3.81	4.40	8.19	10.61	14.71	15.54
	Pleistocene	G/G_{\max}	0.9884	0.9772	0.9139	0.8545	0.6043	0.4640	0.1914	0.1199
		λ (%)	2.90	2.95	3.35	3.85	6.72	8.69	13.07	14.32
Silt sand	Holocene	G/G_{\max}	0.9685	0.9437	0.8078	0.7016	0.3875	0.2668	0.0929	0.0562
		λ (%)	1.00	1.26	2.83	4.13	8.18	9.79	12.15	12.65
	Pleistocene	G/G_{\max}	0.9774	0.9587	0.8499	0.7581	0.4525	0.3210	0.1166	0.0711
		λ (%)	1.38	1.50	2.40	3.30	6.78	8.45	11.18	11.81
Clay	Continental depositional	G/G_{\max}	0.9852	0.9730	0.8968	0.8256	0.5395	0.3926	0.1409	0.0835
		λ (%)	3.81	3.83	4.12	4.58	8.00	10.58	16.16	17.62
	Marine depositional	G/G_{\max}	0.9883	0.9787	0.9181	0.8601	0.6092	0.4659	0.1875	0.1157
		λ (%)	3.45	3.48	3.80	4.20	6.62	8.33	12.17	13.25

As was previously discussed, the soils formed in the Quaternary marine sedimentary environment in the offshore areas of the Yellow Sea have significantly different dynamic shear modulus ratios and damping ratios than those formed in the Quaternary continental sedimentary environment. The effect of geological age on G/G_{\max} is similar to its effect on λ , while the effect on G/G_{\max} is slightly greater than that on λ . For ease of application in practical engineering, the fitting parameters of the $G/G_{\max} \sim \gamma_a$ curves and the $\lambda \sim \gamma_a$ curves were obtained for each type of the classified samples (Table 3). For silty clay and silt, the newer the sedimentary age, the smaller the value of A and the bigger the value of B. The average G/G_{\max} and λ values at various shear strain levels calculated by the recommended parameters are presented in Table 4.

5. Conclusions

The sedimentary characteristics of the Quaternary soils formed during the transgression in the offshore areas of the Yellow Sea were investigated. The dynamic shear modulus ratios and the damping ratios of the soil samples were tested considering the effects of sedimentary environments,

geological ages, and soil types. The main conclusions are as follows.

- (1) The G_{\max} of various marine soils increases with the depth and shows a typical linear relationship
- (2) The effects of marine transgression on the $G/G_{\max} \sim \gamma_a$ and $\lambda \sim \gamma_a$ curves of the Quaternary soils in the offshore areas of the Yellow Sea are significant. The effects are strong on the clays, moderate on the silty clays, and minor on the silts. The $G/G_{\max} \sim \gamma_a$ and $\lambda \sim \gamma_a$ curves of the Pleistocene marine clays are higher and lower than those of the continental clays, respectively, which may be due to the higher strength of the clay crust formed during the marine transgression
- (3) The effects of geological ages on the $G/G_{\max} \sim \gamma_a$ and $\lambda \sim \gamma_a$ curves of the Quaternary soils in the offshore areas of the Yellow Sea have significant differences between soil type. The effects were strong on the marine silty clays, marine silts, and continental silty clays

(4) Compared with the sedimentary environment, geological age generally had greater effect on the $G/G_{\max} \sim \gamma_a$ and $\lambda \sim \gamma_a$ curves of the various types of Quaternary soils in the offshore areas of the Yellow Sea. The fitting parameters of the $G/G_{\max} \sim \gamma_a$ and $\lambda \sim \gamma_a$ curves were obtained for each soil type under different sedimentary environments and geological ages. Moreover, the averaged curves for each type of soil were recommended for the application in practical engineering

Data Availability

The data are generated from experiments and can be available from the corresponding author upon request.

Conflicts of Interest

The authors declare that there are no conflicts of interest regarding the publication of this paper.

Acknowledgments

This work was supported by the research grant from the National Institute of Natural Hazards, Ministry of Emergency Management of China (No. ZDJ2018-11) and National Key Research and Development Program of China (2017YFC1500403).

References

- [1] T. C. Kim and M. Novak, "Dynamic properties of some cohesive soils of Ontario," *Canadian Geotechnical Journal*, vol. 18, no. 3, pp. 371–389, 1981.
- [2] T. Kokusho, Y. Yoshida, and Y. Esashi, "Dynamic properties of soft clay for wide strain range," *Soils and Foundations*, vol. 22, no. 4, pp. 1–18, 1982.
- [3] M. Vucetic and R. Dobry, "Effect of soil plasticity on cyclic response," *Journal of Geotechnical Engineering*, vol. 117, no. 1, pp. 89–107, 1991.
- [4] R. Dobry and M. Vucetic, *Dynamic properties and seismic response of soft clay deposits*. Department of Civil Engineering, Rensselaer Polytechnic Institute, 1987.
- [5] C. Guoxing, L. Xuezhu, D. Zhu, and Q. Hu, "Experimental studies on dynamic shear modulus ratio and damping ratio of recently deposited soils in Nanjing," *Chinese Journal of Geotechnical Engineering*, vol. 28, no. 8, pp. 1023–1027, 2006.
- [6] G. X. Chen, Y. F. Bu, and Z. L. Zhou, "Influence of sedimentary facies and depth on normalized dynamic shear modulus and damping ratio of quaternary soils," *Chinese Journal of Geotechnical Engineering*, vol. 39, no. 7, pp. 1344–1350, 2017.
- [7] D. C. Koutsoftas and J. A. Fischer, "Dynamic properties of two marine clays," *Journal of Geotechnical and Geoenvironmental Engineering*, vol. 106, no. 6, pp. 645–657, 1980.
- [8] K. Liang, G. X. Chen, and Y. He, "An new method for calculation of dynamic modulus and damping ratio based on theory of correlation function," *Rock and Soil Mechanics*, vol. 40, no. 4, pp. 1368–1376, 2019.
- [9] W. B. Yang, Q. Wu, and G. X. Chen, "Dynamic shear modulus prediction method of undisturbed soil in the estuary of the Yangtze River," *Rock and Soil Mechanics*, vol. 40, no. 10, pp. 3889–3996, 2019.
- [10] A. M. Morsy, M. A. Salem, and H. H. Elmamlouk, "Evaluation of dynamic properties of calcareous sands in Egypt at small and medium shear strain ranges," *Soil Dynamics and Earthquake Engineering*, vol. 116, no. Jan., pp. 692–708, 2019.
- [11] Q. Wu, Q. Lu, Q. Guo, K. Zhao, P. Chen, and G. Chen, "Experimental investigation on small-strain stiffness of marine silty sand," *Journal of Marine Science and Engineering*, vol. 8, no. 5, p. 360, 2020.
- [12] K. Senetakis and M. Payan, "Small strain damping ratio of sands and silty sands subjected to flexural and torsional resonant column excitation," *Soil Dynamics and Earthquake Engineering*, vol. 114, pp. 448–459, 2018.
- [13] Y. Shan, J. Chen, X. Ke, and H. Mo, "Resonant column test study of the effect of clay minerals on maximum dynamic shear modulus in marine clay," in *Proceedings of the 7th International Conference on Earthquake Geotechnical Engineering*, pp. 17–20, Roma, Italy, 2019.
- [14] F. Castelli, A. Cavallaro, A. Ferraro, S. Grasso, V. Lentini, and M. R. Massimino, "Static and dynamic properties of soils in Catania (Italy)," *Annals of Geophysics*, vol. 61, no. 2, 2018.
- [15] A. Gluchowski, Z. Skutnik, M. Biliniak, W. Sas, and D. Lo Presti, "Laboratory characterization of a compacted-unsaturated silty sand with special attention to dynamic behavior," *Applied Sciences*, vol. 10, no. 7, p. 2559, 2020.
- [16] T. Feng, Y. Tang, Q. Wang, J. Zhang, and J. Song, "Experimental investigation of dynamic characteristics of subsea sand-silt mixtures," *Advances in Civil Engineering*, vol. 2019, Article ID 5619039, 9 pages, 2019.
- [17] A. Khosravi, A. Hashemi, S. Ghadirianniari, and M. Khosravi, "Variation of small-strain shear modulus of unsaturated silt under successive cycles of drying and wetting," *Journal of Geotechnical and Geoenvironmental Engineering*, vol. 146, no. 7, article 04020050, 2020.
- [18] B. O. Hardin and V. P. Drnevich, "Shear modulus and damping in soils: design equations and curves," *Journal of the Soil Mechanics and Foundations Division*, vol. 98, no. 7, pp. 667–692, 1972.
- [19] P. P. Martin and H. B. Seed, "One-dimensional dynamic ground response analyses," *Journal of the Geotechnical Engineering Division*, vol. 108, no. 7, pp. 935–952, 1982.
- [20] M. B. Darendeli, *Development of a New Family of Normalized Modulus Reduction and Material Damping Curves*, The University of Texas at Austin, Austin, USA, 2001.